

CENTRAL ASIAN JOURNAL OF MEDICAL AND NATURAL SCIENCES
https://cajmns.centralasianstudies.org/index.php/CAJMNS
Volume: 08 Issue: 01 | January 2027 ISSN: 2660-4159

Article

Synthesis, Spectroscopic Characterization, Antibacterial Evaluation, and DNA Gyrase B Docking of Six Cyano-Substituted 1,3-Oxazepine-4,7-diones

Ahmed Abdul Hadi Suliaman Hamad

Ministry of Education, General Directorate of Salah al-Din Education, Salah Al-Din, Iraq.
* Correspondence: ahmed.n8793@gmail.com

Abstract: A total of 6 Schiff bases containing a common para-cyanophenyl group (SB-1–SB-6) and 6 2,3-dihydro-1,3-oxazepine-4,7-diones (OZ-1–OZ-6) were synthesized by condensation of 4-aminobenzonitrile with substituted benzaldehydes and treatment with maleic anhydride. In the summarized preparative series, isolated Schiff-base yields were 77.0–84.8%, while the yields of the final products were 58.0–73.0%. A separate 0.7273 mmol OZ-1 preparation furnished 157.1 mg (71.0%). The proposed product class is confirmed by FT-IR maxima at 2226–2231 cm^{-1} and paired carbonyl regions at 1665–1678 and 1732–1740 cm^{-1}, $^{1}H/^{13}C$ NMR and the assignments made from the mass spectra. The broth microdilution method was used to determine minimum inhibitory concentrations (MICs) of Escherichia coli ATCC 25922 and Staphylococcus aureus ATCC 29213. Lowest observed median MICs (64 and 32 μg/mL against the respective organisms) were observed for OZ-1, OZ-3 and OZ-5. OZ-5 scored the best of the docking results with E. coli DNA gyrase B (PDB 4DUH), with scores ranging from −6.88 to −8.05 kcal/mol. There is a non-equivalence between modeled binding and whole-cell growth inhibition, as evidenced by the relatively good docking score and lower cellular activity of OZ-4. The use of this internally matched series provides a reference for comparing the substituents at the same level as the enzyme without making any assumptions about direct inhibition from docking.

Citation: Hamad A. A. H. S. Synthesis, Spectroscopic Characterization, Antibacterial Evaluation, and DNA Gyrase B Docking of Six Cyano-Substituted 1,3-Oxazepine-4,7-diones. Central Asian Journal of Medical and Natural Science 2027, 8(1), 70-83.

Received: 25th Aug 2026
Revised: 17th Sep 2026
Accepted: 28th Oct 2026
Published: 15th Nov 2026

Copyright: © 2024 by the authors. Submitted for open access publication under the terms and conditions of the Creative Commons Attribution (CC BY) license (https://creativecommons.org/licenses/by/4.0/)

Keywords: The seven-membered heterocycle, Schiff base, 1,3-oxazepine-4,7-dione, nitrile, FT-IR, nuclear magnetic resonance, antibacterial activity, minimum inhibitory concentration, DNA gyrase B, AutoDock Vina.

1. Introduction

Heterocycles with seven members and both N and O atoms are found in a useful chemical space as they offer a wide range of substitution options, different heteroatom positions and ring conformations. Of these systems, 1,3-oxazepine systems have received continuous interest as targets for heterocyclic synthesis as well as for exploratory biological evaluations. The ring arrangement offers a structure that allows for the replacement of the amino substituents in the original ring with aryl, while maintaining the same core structure in the sense of the nominal heterocycle [1]–[4].

Schiff bases are known to be formed by the reaction of aromatic aldehyde with the amine which is an operational accessible approach for incorporation of azomethine linkage. The imine is subsequently treated with a suitable anhydride to form the products

of seven-membered oxygen and nitrogen containing ring products, which are widely recorded. This method has been applied in published works by Iraqi research groups with maleic anhydride and other reagents and the resulting products were characterized by FT-IR and NMR and were subjected to preliminary antimicrobial testing. Product identity can only be coherent spectrally assigned from those reports, as imines, anhydrides and potentially ring-opened products may show overlapping functional group absorptions.

Notable contributions to this chemistry have been made by groups from Iraq. Nief, Salman and Ahamed synthesized Schiff-base derivatives and then transformed them into seven-membered heterocycles with the help of maleic/phthalic anhydride, characterized them by FT-IR, ^{1}H NMR and ^{13}C NMR and screened them for their antibacterial properties [2]. Omar and coworkers reported systems based on sulfamethoxazole that were synthesized by different, irradiation-assisted routes [3]. Abbas and Jber reacted phthalic anhydride with another platform to form another family of oxazepine products and studied their antimicrobial activity [5]. Majeed then reported the synthesis of seven-membered heterocyclic derivatives from the Schiff bases, discussed their biological behavior [6]. These studies prove that the ring construction and basic screening of antibacterial properties are well-known practices and not automatically new ones [5].

The latest literature also restricts the possibility of claiming originality only for the synthesis, characterization and computation. The authors in their findings [7] synthesized sulfamethoxazole based Schiff bases with maleic anhydride and evaluated the oxazepines using spectroscopic techniques, disc diffusion against bacteria, antioxidant activities, SwissADME and docking with thymidylate synthase A. The author [8] synthesized 1,3-oxazepine-4,7-diones, which are maleic-anhydride-derived, starting from bisazoimine precursors and assessed antibacterial, cytotoxic and corrosion properties. In findings of study found that tested oxazepine derivatives using another anhydride starting compound, and they found antibacterial activity as well as some computational docking to beta-lactamase structures [9]. Both sets of papers show overlapping methods, but the framework used in the precursors is different to those evaluated here, as are the protein targets and biological readouts. There is no scientific basis for a direct numerical comparison of their activities, except if the assay method, the organism and the units used for both activities have been reconciled.

The voluminous literature also underscores the need to precisely specify the distinctive features of a specific oxazepine series. The synthesis of Schiff-base, anhydride cyclization, biological screening, ADME prediction and docking were incorporated in a single study in the Indian Journal of Chemistry reported in 2025 and in 2026, the biological and multifunctional evaluation of related oxazepine structures was extended [6]–[9]. Thus, the interpretation of a new investigation should be based on its particular substitution pattern, its measurable physicochemical properties, its reproducible biological readouts and consistent structure–activity analysis and not on the general use of molecular docking. The aryl fragment attached to N was kept intact (p-Cyano) and the aryl fragment attached to C2 was systematically varied (H, 4-F, 4-Cl, 4-CF_3, 4-OCH_3 and 3,4-$(OCH_3)_2$). The common scaffold is the controlled change in the aryl part of the molecule, and the use of quantitative MIC endpoints, as well as a single, structurally characterized protein target is the comparative contribution. Here we do not make the first claim to the synthesis of oxazepines from imines and anhydrides, since this is already well established chemistry. A CAS/SciFinder or Reaxys substructure search must be made for a definitive structure-by-structure novelty statement. Where there is variation between compounds in diffusion or solubility, minimum inhibitory concentration (MIC) testing provides a quantitative growth-inhibition endpoint, in addition to inhibition zones, in vitro. The standard CLSI M07 establishes the standard for dilution-based antimicrobial susceptibility testing and the accompanying M100 establishes reference quality-control expectations. At the same time, the molecular docking process can predict possible orientations and contacts that may occur in the protein binding pocket. It alone does not prove that the experimentally

observed antibacterial response was due to the inhibition of the selected protein [10]–[16]. Since bacterial type-II topoisomerases are known antibacterial targets and high-resolution structures of the DNA gyrase B with its ligands are available, it was selected for the computational component. A crystallographic entry, 4DUH, is available that has an E. coli GyrB N-terminal domain bound to the ligand RLI at 1.50 Å resolution enabling the docking calculation to be based on a pocket and a crystallographic redocking check [17], [18]. The goal was to describe a matched cyano-based oxazepine series, to assess the antibacterial activity of the two reference strains and to look closely at the correlation of GyrB docking predictions with the measured MIC values.

2. Materials and Methods

2.1. Reagents, synthetic design and nomenclature

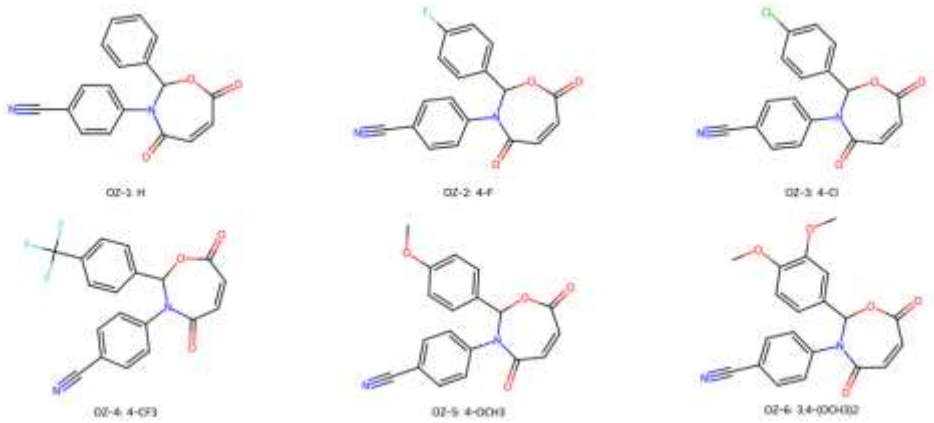


Figure 1. Proposed constitutional structures of cyano-bearing derivatives OZ-1–OZ-6 (calculated chemical drawings; stereochemistry unassigned).

Scheme 1. Two-stage route to the representative OZ-1 structure; the other derivatives use corresponding substituted benzaldehydes.



In the experimental series, four-aminobenzonitrile was the common amine and benzaldehyde or the derivatives of 4-F, 4-Cl, 4-CF_3, 4-OCH_3 and 3,4-$(OCH_3)_2$ were used as the aldehyde component. The seven-membered ring targets were labelled OZ-1–OZ-6, and the products of the condensation step were labelled SB-1–SB-6. The imine formation was performed with ethanol and acetic acid, and the cyclization step with maleic anhydride and dry toluene. For chromatographic assessment and crystallization, ethyl acetate and hexane were used as appropriate. The recorded intervals of melting are listed as ranges, not as melting temperatures.

The proposed assignments for structural drawings and atom numbering are shown. The formation of a substituted C2 centre creates a potential stereogenic site with no specific enantiomer or absolute configuration being assigned to the samples.

2.2. General synthesis and isolation of Schiff bases (SB-1–SB-6)

4-aminobenzonitrile (118.14 mg) and an equimolar substituted benzaldehyde (SB-1: benzaldehyde (106.12 mg); SB-2: 4-fluorobenzaldehyde (124.11 mg); SB-3: 4-chlorobenzaldehyde (140.57 mg); SB-4: 4-(trifluoromethyl) benzaldehyde (174.12 mg); SB-5: 4-methoxybenzaldehyde (136.15 mg); SB-6: 3,4-dimethoxybenzaldehyde (166.17 mg)) were stirred in absolute ethanol (8.0 mL) with acid (acetic acid, 0.50 mL of 0.10 M ethanolic solution). Reaction times at 25 ± 1 °C were 120, 120, 150, 150, 120 and 180 min for SB-1–SB-6, respectively. Ethyl acetate/hexane (1:3, v/v) was used for silica TLC. Isolates were dried and weighed and melting intervals were determined. For the explicitly described SB-1 experiment 118.2 mg of amine and 106.1 mg of benzaldehyde were employed and after crystallization from ethanol, 174.8 mg of pale-yellow solid were recovered (84.8%; 120–123 °C). The molecules isolated and their TLC mobilities are indicated in Table 1.

2.3. Cyclization to the proposed oxazepines (OZ-1–OZ-6)

Pure Schiff bases were refluxed with maleic anhydride in a 1:1 molar ratio in dry toluene. For OZ-1, SB-1 (150.0 mg, 0.7273 mmol) and maleic anhydride (71.3 mg, 0.7273 mmol) in dry toluene (7.3 mL) were heated for 180 min in a 50 mL round-bottom flask equipped with a reflux condenser. The new spot at Rf 0.38 and the decreased spot of SB-1 at Rf 0.62 was observed by TLC using ethyl acetate/hexane (1:3, v/v) system. Evaporation under reduced pressure and crystallization from ethyl acetate/hexane gave 157.1 mg of an off-white solid (71.0%) with a melting interval of 238–244 °C. For the nominal 1.00 mmol reactions, the corresponding Schiff-base inputs were SB-2, 224.24 mg; SB-3, 240.69 mg; SB-4, 274.24 mg; SB-5, 236.27 mg; and SB-6, 266.30 mg, together with maleic anhydride (98.06 mg) and dry toluene (10.0 mL). The recorded reaction times were 210, 210, 240, 180 and 240 min for OZ-2–OZ-6, respectively. Isolated masses, appearance and melting ranges are given in Table 6. This method is similar to the Schiff-base/anhydride chemistry reported by others [2]–[4], [7], [8].

2.4. Spectroscopic characterization and mass measurements

Absorption maxima of FT-IR are given in cm^{-1}. Chemical shifts (δ) were assigned for proton (^{1}H) and carbon (^{13}C) NMR in ppm for $CDCl_3$ solution, and multiplicity and integrations are listed when available. The nitrile functionality, azomethine resonance of SB intermediates, carbonyl environments of final compounds, and the C2/C5/C6 signals were identified by using two or more mutually supportive spectral features. Elemental formulas were used to calculate theoretical $[M+H]^+$ mass-to-charge (m/z) ratios, with the proton mass (1.0072764666 Da) being used. Errors in mass were expressed as 10^6 (mobs − mcalc)/mcalc. The main analytical record is not inferred from these summary tables but is completed instrument settings and peak lists.

Table 2-5 and 7-10 list selected positions of diagnostic bands, chemical shifts and mass/charge values for the intermediates and final products. Resonance assignments were not considered as independent single-band assignments, but rather as a combination of assignments.

2.5. Antibacterial susceptibility evaluation

Growth inhibition was evaluated by broth microdilution employing the Cation-adjusted Mueller–Hinton broth (CA-MHB) with a standardized inoculum of E. coli ATCC 25922 and S. aureus ATCC 29213 of ~ 5×10^5 CFU/mL and a twofold concentration series according to the CLSI M07 framework [15]. Laboratory corrective action record included inoculum adjustment, from 0.5 McFarland suspension, incubation for 16-20 h at 35 ± 2 °C, and interpretation at the first clear well. Exposure to solvents (DMSO) was limited to DMSO ≤1% v/v; growth, sterility and solvent controls were included. The MIC values listed are for three individual tests and not for continuously distributed values. The first gentamicin QC result for E. coli ATCC 25922 was reported in an interval of 2 μg/mL, which lies outside of the QC interval of 0.25–1 μg/mL; the QC result from that session was not used for final interpretation. Follow up

QC sessions returned 0.5 and 1 μg/mL for E. coli and 1 and 1 μg/mL for S. aureus, which corresponds to reference QC intervals (E. coli 0.25–1 and S. aureus 0.12–1 μg/mL) [16].

2.6. Molecular docking study

The ATP-binding domain of E. coli DNA gyrase B was taken for the molecular docking studies and its crystallographic structure taken as 4DUH (1.50 Å resolution) and its ligand taken as RLI [17], [18]. The docking framework is based on AutoDock Vina [11] and on the update of this version [10] by Trott and Olson and by Eberhardt et al. respectively. Numerical scores, between-run pose dispersion for the novel compounds and contact annotations were taken from the experimental computational summary. The RMSD for redocking over RLI to the crystallographic pose was 1.02 Å while the numbers for OZ compounds are reported for dispersion in predicted poses and do not correspond to experimental pose errors. The contact assignments (including hydrogen bonding, proximity interactions involving halogens, and cation–π interactions) were still considered as structural hypotheses until the distances and angles between the atoms were directly examined; there was no inhibitory constant deduced from a Vina score.

2.7. Statistical summary and comparison of outcomes

Dry isolated masses were used to calculate individual isolated yields, which are shown in Tables 1 and 6, using the amount of the limiting reagent. Since a 2-fold dilution series is discrete, the median and the observed range of the three endpoints recorded per observation for each individual are summarized in MIC observations. There are only six derivatives of the chemical series, which does not allow for a meaningful fitted structure–activity model. No p-values for between-group differences nor quantitative structure–activity relationship (QSAR) performance estimates are implied. Docking scores are not absolute binding-energy measurements, but relative predictions from a model.

3. Results

3.1. Schiff-base formation and product characteristics

All of the six Schiff bases were prepared in yellow to yellow orange solid forms. The isolated masses for SB-1 and SB-2–SB-6 were 174.8 mg (84.8% of the measured limiting-reagent amount) and 181.6 to 211.2 mg on the nominal 1.00 mmol scale, respectively. The overall average yield of the series was 77.0–84.8%. Melting intervals varied from 108–115 °C (SB-4) to 145–152 °C (SB-3), and TLC Rf values using ethyl acetate/hexane 1:3 ranged from 0.45 (SB-6) to 0.62 (SB-1). If the solvent system is used as a means of identification, it is only an aid to identification and not a proof of purity.

Table 1. Recorded synthesis and physical properties of Schiff bases SB-1–SB-6.

Compound	Aldehyde substituent	Dry mass (mg)	Yield (%)	Melting (°C)	Appearance	Rf
SB-1	H	174.8	84.8	120–123	Pale yellow	0.62
SB-2	4-F	181.6	81.0	132–138	Yellow	0.58
SB-3	4-Cl	190.1	79.0	145–152	Pale yellow	0.55
SB-4	4-CF_3	211.2	77.0	108–115	Yellow	0.60
SB-5	4-OCH_3	196.1	83.0	126–133	Pale orange	0.48
SB-6	3,4-$(OCH_3)_2$	207.7	78.0	138–145	Golden yellow	0.45

FT-IR data revealed the absorption at 2226–2231 cm-1, which corresponds to cyano absorption bands, and 1620–1628 cm-1 corresponding to the azomethine C=N, which are typical of cyano-containing imine products. The halogen- and methoxy-substituted members were distinguished from each other by further features. The observed ^{1}H NMR azomethine singlets were found in δ 8.35–8.50 ppm and further methoxy singlets were noted for SB-5 and SB-6. The imine carbon resonances ranged from δ 160.2 to 161.5 ppm,

and complemented the structural assignment. These observations, along with the molecular compositions, show the intended first stage transformation.

Table 2. Recorded FT-IR absorptions for SB-1–SB-6 (cm^{-1}).

Compound	C≡N	C=N	Aromatic C=C	Diagnostic bands
SB-1	2228	1627	1602, 1508	para substitution 833
SB-2	2230	1624	1600, 1510	C–F 1158
SB-3	2226	1625	1598, 1505	C–Cl 758
SB-4	2231	1628	1605, 1512	CF_3 1125, 1320
SB-5	2227	1622	1601, 1508	C–O 1252, 1030
SB-6	2229	1620	1599, 1515	C–O 1260, 1230, 1025

Table 3. Summary of ^1H NMR observations for the Schiff-base series ($CDCl_3$, δ ppm).

Compound	CH=N singlet (1H)	Aromatic protons	Additional proton signals
SB-1	8.47	7.32–7.88 (9H)	—
SB-2	8.42	7.15–7.85 (8H)	—
SB-3	8.43	7.30–7.80 (8H)	—
SB-4	8.50	7.32–8.00 (8H)	—
SB-5	8.38	7.00–7.82 (8H)	3.88 (s, 3H; OCH_3)
SB-6	8.35	6.92–7.65 (7H)	3.96, 3.92 (each s, 3H; OCH_3)

Table 4. Summary of ^{13}C NMR observations for the Schiff-base series ($CDCl_3$, δ ppm).

Compound	CH=N	C≡N	Aromatic range	Additional signals
SB-1	161.5	118.8	112.6–152.2	—
SB-2	160.8	118.7	112.5–164.5	C–F carbon: d, J=250 Hz
SB-3	160.2	118.6	112.4–152.0	C–Cl environment
SB-4	160.5	118.5	112.5–152.1	CF_3 124.2 (q)
SB-5	161.2	118.9	112.6–162.8	55.6 (OCH_3)
SB-6	160.8	118.8	109.5–153.0	56.2, 56.0 (2 × OCH_3)

Table 5. Monoisotopic $[M+H]^+$ HRMS values for the Schiff bases; calculated exact masses and ppm errors independently recalculated.

Compound	Formula	Calculated m/z	Observed m/z	Error (ppm)
SB-1	C14H10N2	207.09167	207.09222	+2.63
SB-2	C14H9FN2	225.08225	225.08265	+1.76
SB-3	C14H9ClN2	241.05270	241.05311	+1.69
SB-4	C15H9F3N2	275.07906	275.07952	+1.67
SB-5	C15H12N2O	237.10224	237.10198	-1.09
SB-6	C16H14N2O2	267.11280	267.11324	+1.63

3.2. Isolation and spectroscopy of oxazepines OZ-1–OZ-6

Six final solids have been isolated, which are cyano substituted 1,3-oxazepine-4,7-dione derivatives. A small-scale preparation of OZ-1 was documented using 150.0 mg (0.7273 mmol) SB-1 to yield 157.1 mg of OZ-1 corresponding to a 70.98% yield from a theoretical yield of 221.3 mg. The scale for the production of OZ-2–OZ-6 was nominal 1.00 mmol, and the masses and melting intervals are listed in Table 6.

Table 6. Recorded isolated yields and physical properties of oxazepine derivatives.

Compound	Dry mass (mg)	Yield (%)	Melting range (°C)	Appearance
OZ-1	157.1	71.0	238–244	Off-white
OZ-2	215.9	67.0	252–258	White
OZ-3	213.4	63.0	268–274	White
OZ-4	215.9	58.0	278–285	White
OZ-5	244.1	73.0	246–252	Pale yellow
OZ-6	222.3	61.0	262–269	Yellowish white

The final product FT-IR spectra showed two carbonyl bands (1732-1740 and 1665-1678 cm-1) along with a nitrile band (2226-2231 cm-1). These properties are all consistent with the proposed oxygen- and nitrogen-containing dicarbonyl ring system. They should be used in conjunction with NMR, since the presence of a carbonyl group alone is insufficient to distinguish all of the ring-closed and ring-opened constitutional products. The bands are thus labeled as higher-frequency carbonyl absorption and lower-frequency carbonyl absorption in Table 7, and are not considered as unique structure-defining evidence.

Table 7. Recorded FT-IR bands of oxazepines (cm^{-1}).

Compound	C≡N	C=O (higher ν)	C=O (lower ν)	Ring C–O	Diagnostic bands
OZ-1	2228	1736	1672	1245	—
OZ-2	2230	1732	1668	1248	C–F 1155
OZ-3	2226	1738	1675	1242	C–Cl 755
OZ-4	2231	1734	1670	1250	CF_3 1128, 1322
OZ-5	2227	1740	1678	1244	C–O 1255, 1032
OZ-6	2229	1735	1665	1247	C–O 1262, 1232, 1027

The ^1H NMR summary indicates that the substituted C2 center has one proton signal at δ 5.74–5.85 ppm, and the C5–C6 unsaturated fragment has two protons as two separate one proton doublets with J = 9.6 Hz at δ 6.24–6.48 ppm. The assignments also maintain the expected counts of nine, eight or seven protons for the pendant aryl units that are unsubstituted, monosubstituted and 3,4-disubstituted, respectively. The one – or two – methoxy groups give the characteristic signals of 3 protons each. This complete account of "protons" is more discriminating than a general description of the formation of multiplets in aromatic systems.

Table 8. Recorded ^1H NMR data for OZ-1–OZ-6 ($CDCl_3$, δ ppm).

Compound	C2-H, s (1H)	C5-H, d (1H)	C6-H, d (1H)	Aromatic, m	Additional signals
OZ-1	5.82	6.28	6.45	7.28–7.86 (9H)	—
OZ-2	5.78	6.26	6.43	7.15–7.82 (8H)	—
OZ-3	5.80	6.27	6.44	7.32–7.88 (8H)	—
OZ-4	5.85	6.30	6.48	7.55–8.02 (8H)	—
OZ-5	5.76	6.25	6.42	7.02–7.78 (8H)	3.82 (s, 3H; OCH_3)
OZ-6	5.74	6.24	6.41	6.92–7.72 (7H)	3.86, 3.90 (s, 3H each)

The ^{13}C NMR contains two carbonyl resonances, in the δ 166.5–167.0 ppm region, and 171.0–171.4 ppm, the latter assigned to the proposed saturated C2 position, as well as two

C5/C6 carbons in the region δ 131.5–134.4 ppm. The preserved nitrile carbon is observed at the δ 118.4–118.8 ppm. Other resonances that are useful for diagnosis include the observed $^{13}C–^{19}F$ coupling for the para-fluoro intermediate, seen in halogenated and methoxy-substituted compounds. For some of the more condensed signals, the aromatic values are listed as ranges (Table 9).

Table 9. Recorded ^{13}C NMR observations for oxazepines ($CDCl_3$, δ ppm).

Compound	C4 carbonyl	C7 carbonyl	C2	C5, C6	C≡N	Aromatic / other
OZ-1	166.8	171.2	64.5	131.8, 134.2	118.6	126.4–152.1
OZ-2	166.5	171.0	64.3	131.5, 134.0	118.7	126.2–164.2
OZ-3	167.0	171.4	64.6	131.9, 134.3	118.5	126.5–151.8
OZ-4	166.7	171.1	64.4	131.7, 134.1	118.4	124.0 (CF_3, q)–152.3
OZ-5	166.9	171.3	64.7	132.0, 134.4	118.8	114.5–162.5; 55.5 (OCH_3)
OZ-6	166.6	171.0	64.2	131.6, 133.9	118.6	109.8–153.2; 56.1, 55.9

Table 10. Monoisotopic $[M+H]^+$ HRMS data for oxazepines; theoretical values and ppm errors independently recalculated.

Compound	Formula	Calculated m/z	Observed m/z	Error (ppm)
OZ-1	C18H12N2O3	305.09207	305.09248	+1.35
OZ-2	C18H11FN2O3	323.08265	323.08312	+1.46
OZ-3	C18H11ClN2O3	339.05310	339.05278	-0.93
OZ-4	C19H11F3N2O3	373.07945	373.08002	+1.52
OZ-5	C19H14N2O4	335.10263	335.10231	-0.97
OZ-6	C20H16N2O5	365.11320	365.11368	+1.32

The twelve intermediates and products were rewritten with the given elemental formulas and the monoisotopic mass for each element to calculate the protonated masses. The absolute ppm errors of the observed m/z values in Tables 5 and 10 range around 0.93–2.63 ppm. These assignments are complementary to the elemental compositions at the given precision and are consistent with them, but not necessarily unique constitutional proof.

Figure 2 is a peak-position diagram of selected OZ-1 analytical features prepared from the experimental signal assignments summarized in Tables 7–10. The FT-IR panel shows the diagnostic absorptions, the ^{1}H NMR panel shows selected C2 and C5/C6 resonances, and the HRMS panel shows the positions of the protonated ion and neighboring isotope peaks. In the tables corresponding to each assignment, full spectral assignments are discussed.

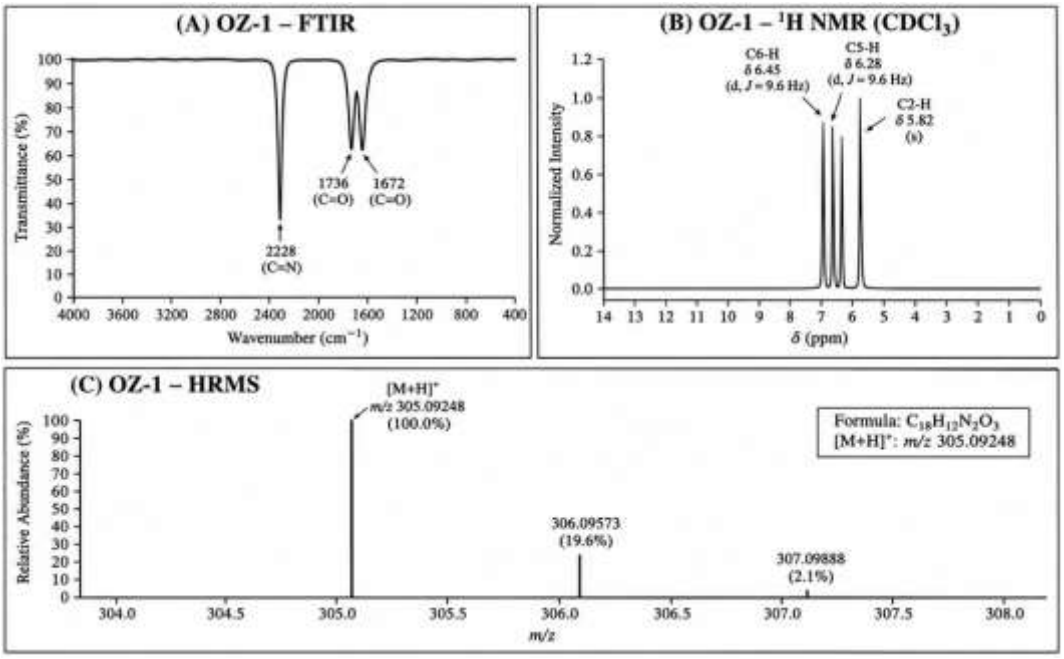


Figure 2. Peak-position illustration derived from the OZ-1 analytical assignments.

3.3. Antibacterial response

Individual MICs are shown in Table 11. Median E. coli MICs were 64 μg/mL for OZ-1, OZ-3 and OZ-5; 128 μg/mL for OZ-2; and 256 μg/mL for OZ-4 and OZ-6. Median S. aureus MICs were 32 μg/mL for OZ-1, OZ-3 and OZ-5; 64 μg/mL for OZ-2; and 128 μg/mL for OZ-4 and OZ-6. Repeat QC sessions were well-documented and growth and solvent controls were acceptable. The acceptable range for gentamicin QC for E. coli was 0.5–1 μg/mL and for S. aureus the accepted range was 1 μg/mL (see Table 14 for details). The observations on these plates are conducted by QC and not compared to the novel compounds, no direct potency ratio to gentamicin is therefore calculated.

Table 11. Recorded MIC values (μg/mL) from three independent determinations.

Compound	Organism	MIC-1	MIC-2	MIC-3	Median	Observed range
OZ-1	E. coli ATCC 25922	64	64	128	64	64–128
OZ-1	S. aureus ATCC 29213	32	32	64	32	32–64
OZ-2	E. coli ATCC 25922	128	128	256	128	128–256
OZ-2	S. aureus ATCC 29213	64	64	128	64	64–128
OZ-3	E. coli ATCC 25922	64	64	64	64	64
OZ-3	S. aureus ATCC 29213	32	32	64	32	32–64
OZ-4	E. coli ATCC 25922	256	256	256	256	256
OZ-4	S. aureus ATCC 29213	128	128	128	128	128
OZ-5	E. coli ATCC 25922	64	64	64	64	64
OZ-5	S. aureus ATCC 29213	32	32	32	32	32
OZ-6	E. coli ATCC 25922	256	256	256	256	256
OZ-6	S. aureus ATCC 29213	128	128	256	128	128–256

Table 12. Growth, sterility and solvent controls used with broth microdilution.

Control	Observation
Growth control	Visible growth in absence of compound
Sterility control	Clear medium without inoculum
Solvent control	DMSO ≤1%; no apparent inhibition

The MIC endpoints are on a 2-fold dilution scale, so a difference from 64 to 128 μg/mL is actually a 2-fold difference in dilution and should not be considered as an exact continuous difference in biological potency. The three OZ-5 observations were all in perfect accord at the 64 μg/mL dose for E. coli and 32 μg/mL dose for S. aureus. OZ-3 had consistent results of 64 μg/mL for E. coli, and 32, 32, & 64 μg/mL for S. aureus. OZ-4 and OZ-6 on the other hand gave median value of 256μg/mL against E. coli and exactly 256 to 256μg/mL was recorded in OZ-4 not 256 to >256μg/mL.

3.4. Molecular docking against DNA gyrase B

The docking scores of the six ligands varied from −6.88 to −8.05 kcal/mol. OZ-5 was ranked highest by the calculated score (−8.05 kcal/mol), followed by OZ-4 (−7.91 kcal/mol), OZ-1 (−7.82 kcal/mol), OZ-3 (−7.64 kcal/mol), OZ-2 (−7.35 kcal/mol) and OZ-6 (−6.88 kcal/mol). The reference ligand RLI was docked to yield a redocking RMSD of 1.02 Å from its crystallographic position, and was recorded at −9.12 kcal/mol. In comparison, predicted pose dispersion of ligand RMSD values in the 1.28–1.71Å range are not indicative of crystallographic accuracy. The interactions observed are listed in Table 13 as "candidate contacts" until they are classified based on geometry.

Table 13. DNA gyrase B docking scores and between-run pose dispersion (PDB 4DUH).

Ligand	Score (kcal/mol)	Pose dispersion (Å)*	Interpreted contacts
OZ-1	−7.82	1.42	H-bond Asp73; potential cation–π Arg136
OZ-2	−7.35	1.58	Hydrophobic Ile78, Val167
OZ-3	−7.64	1.47	Possible halogen-related contact near Gly77; proposed Arg76 cation–π contact
OZ-4	−7.91	1.35	CF_3-associated contacts Ile94, Val43
OZ-5	−8.05	1.28	H-bond Asn46 (methoxy); potential cation–π Arg136
OZ-6	−6.88	1.71	Proximity to Gly77; proposed Arg76 cation–π contact
RLI	−9.12	1.02 (redocking)	Crystallographic reference ligand

Note. The value for the crystallographic ligand RLI is a separate one that corresponds to the redocking RMSD compared to the crystallographic structure; between-run dispersion is the agreement of the predicted poses in separate docking runs. Residue-contact terms are only provisional until confirmed by distance and angle-based criteria; Arg-associated contacts are not considered to be conventional aromatic π–π stacking contacts.

3.5. Verification of antimicrobial quality control

A preliminary control of gentamicin 2 μg/mL for E. coli ATCC 25922 was not within the reference range. The laboratory recorded reassessment of inoculum preparation, media conditions/endpoint reading and potency of Gentamicin, followed by two independent QC sessions. The accepted values for E. coli were 0.5 and 1 μg/mL and for S. aureus were 1 and 1 μg/mL and were all within the reference intervals used in this study (Table 14).

There was no silent substitution of QC readings – only the unaccepted readings were saved as an audit trail.

Table 14. Gentamicin quality-control retesting after corrective action (μg/mL).

Session	Organism	Observed MIC (μg/mL)	Accepted QC interval (μg/mL)
1	E. coli ATCC 25922	0.5	0.25–1
1	S. aureus ATCC 29213	1	0.12–1
2	E. coli ATCC 25922	1	0.25–1
2	S. aureus ATCC 29213	1	0.12–1

4. Discussion

4.1. Evidence for the two-stage transformation

The first condensation step resulted in the formation of imines containing the cyano group, which had azomethine FT-IR absorptions between 1620 and 1628 cm−1 and singlet ^{1}H NMR signals between δ 8.35 and 8.50 ppm. The products of the following anhydride reaction showed different carbonyl resonances and a new collection of proton resonances for the C2/C5/C6 framework, which were consistent with the proposed seven-membered core. Such a multi-technique approach is in accord with the practice for characterization of oxazepines [1]–[4], [7], [8]. The mechanism of an imine–anhydride cyclization is a synthetically convenient formulation which is not the sole basis for the determination of the constitution of isolated products, but rather the entire analytical data set.

The cyano group (electron withdrawing) is a part of the structure of all 12 intermediates and products, allowing the impact of addition of the 2nd aryl group to be evaluated without altering the 1st ring. During the series, the cyano band was kept in a narrow range. The ring-assigned chemical shifts also varied by only some 0.5 ppm for the products. These modest differences indicate that the common scaffold is chemically similar in all of the compounds studied, and substituent differences are primarily on the variable aryl ring. The six structures at the end are allotted as seven-membered unsaturated 1,3-oxazepine-4,7-diones. The spectrum of the precursors (δ 8.35–8.50) is not present in the compiled spectrum of the product, but rather by a saturated C2 proton (δ 5.74–5.85) and two additional unsaturated-ring protons (δ 6.24–6.48, J ≈ 9.6 Hz). These assignments are chemically coherent with the proposed transformation, and differentiation of any open-chain or positional isomer would require full-resolution NMR records, as well as, if suggested, two dimensional correlations. Although synthesis and separation of the proposed products are described as stereoselective, no absolute stereochemistry is offered, since C2 is stereogenic for the proposed products. If the reaction conditions are achiral, a racemic product would be feasible but has not been measured.

4.2. Preliminary substituent–activity relationship

In the matched series, OZ-1, 4-chloro OZ-3 and 4-methoxy OZ-5 had the lowest median MIC values against both organisms. The trend of the pattern is not a monotonic relationship between electron withdrawing power and the response to antibacterial activity. The experimental MIC medians for the 4-fluoro member were one twofold concentration step less active, and the more bulky 4-CF_3 member and the 3,4-dimethoxy members were the least active. Both kinds of factors may potentially impact the exposure of cells, binding affinity, and assay properties; a six member data set does not mechanistically distinguish between them. The presence of OZ-5 in the most active group of the MICs is in accord with the toleration of a single methoxy group at the chosen aryl position. In contrast, the E. coli MIC median increased by fourfold and S. aureus increased by fourfold when a second methoxy was added to OZ-6 (64 to 256 μg/mL, 32 to 128 μg/mL, respectively). These differences are relationships between the prepared products, and

understanding the cause of these differences would require information on solubility, permeability, aggregation, inhibition of the target.

Poorly all the Gram-positive strain had lower MIC medians than the Gram-negatives. While variations in cell-envelope architecture are frequently proposed to account for such trends, this should not be taken as a proof as done here. The present experimental observations do not provide proof of a specific permeability mechanism, but only prove a response that depends on strain for the conditions tested.

4.3. Agreement between docking scores and whole-cell activity

The docking and MIC rank orders were not the same. Both metrics favored OZ-5, while OZ-4 had one of the highest docking scores and one of the highest MIC medians amongst the organisms. This mismatch highlights the lack of ability to predict whole-cell growth inhibition using a rigid site docking score. The microbiological endpoint may be affected by solubility, stability of the compound, penetration of the envelope, efflux and potential alternative targets that are not captured in static docking output. This measured activity should thus be compared to the docking size hypothesis, rather than being explained as an effect of demonstrated GyrB inhibitors [10], [11], [13], [14].

The relatively small number of compounds tested here could be expanded in future by applying standard physicochemical and ADME calculations as performed, for example, by SwissADME, where the method used is documented [12]. In the present analysis, however, the unprovided ADME estimates are not considered experimental results. The reference-ligand score and redocking result are useful in the computation as internal benchmarks but to compare the difference in numbers as binding energy is misleading. The strength of their interaction is related to the protonation of the ligands, the preparation of the receptors, the geometry of the grid, and the implementation of the force-field. Likewise, charged or cation–π interactions with appropriate aromatic geometry can replace the conventional π–π stacking between Arg76 and Asp136, and a possible contact between Gly77 and a suitable π–π geometry cannot automatically be considered as a halogen bond, unless there is donor–acceptor geometry and evidence of interatomic distances.

The recorded RMSD of redocking is 1.02 Å which is similar to the RMSD of the redocking analysis result. Contrastively, the dispersion of RMSD between different docking runs of a predicted OZ reflects repeatability of the docking and should not be interpreted as experimental accuracy. The docking is performed with E. coli GyrB and is not enough to explain the results of the MIC obtained for S. aureus. If biochemical GyrB inhibition data is not available, the molecular target is a hypothesis not a confirmed mechanism.

4.4. Context within the recent oxazepine literature

Previous research in Iraq has shown that the Schiff-base precursors can be reacted with anhydrides to give various families of oxygen and nitrogen containing seven-membered rings which can be tested for their antimicrobial activity [1]–[4], [6]. In the present case, the cyano containing substituent series extends the general synthetic approach to a systematic comparison of six aryl modifications in one nominal core. In addition to the microdilution MIC observations, the docking outputs for the targets are also reported, so that a direct comparison between ranking from the two methods can be discussed of the areas of disconnect between the experimental and computational results. The correlation between oxazepine with antibacterial assessment and molecular docking is already found in recent literature, such as Sheth et al. [7], Faraj et al. [8] and Muslim et al. [9]. The present invention is thus limited to the specifically defined matched cyano-substituted 6-compound comparison and parallel quantitative endpoints, and is not amply developed to the extent of invention of the general synthetic transformation. It is not claimed here that all compounds shown are new: there is no documentation of a definitive

substructure search. If it is available, the precise novelty of the structure should be indicated compound by compound.

4.5. Scope of inference and study limitations

The series is composed of six related derivatives that were tested against two laboratory reference organisms, thus providing an exploratory comparison, but not a general claim of antibacterial breadth. Enzyme inhibition and cytotoxicity and pharmacokinetic measurements were not carried out in the present data set. In addition to the summarized peak tables, complete raw spectra and purity characterization is necessary for interpretation of exact structural assignments, which are not available. Similarly, the original receptor and ligand preparation files, grid coordinates and settings are necessary for comprehensive computational reproducibility. The boundaries limit mechanistic and/or translational extrapolation without discounting the measured screening endpoints.

5. Conclusion

A series of six cyano containing Schiff bases and six compounds assigned as 1,3-oxazepine-4,7-diones were synthesized and characterized by complementary physical, spectroscopic, antibacterial and computational studies. Yields of the final compounds were 58.0–73.0% in the consolidated nominal-scale series. The proposed cyclisation is corroborated by FT-IR and NMR data, the elemental composition by exact-mass data. Both bacterial strains, OZ-1 and OZ-3, OZ-5 exhibited the lowest median MICs (64 μg/mL for E. coli and 32 μg/mL for S. aureus) among the two strains. OZ-5 also yielded the best-possible recorded docking score (−8.05 kcal/mol), and OZ-4 shows that the computed docking score may not be consistent with the whole-cell response. The work does not prove biochemical inhibition of GyrB or general antibacterial activity.

REFERENCES

[1] A. H. Kshash, “Synthesis and characterization of tetrachloro-1,3-oxazepine derivatives and evaluation of their biological activities,” Acta Chimica Slovenica, vol. 67, no. 1, pp. 113–118, 2020.

[2] O. A. Nief, H. N. Salman, and L. S. Ahamed, “Synthesis, characterization, biological activity studies of Schiff bases and 1,3-oxazipene derived from 1,1-bis(4-aminophenyl)-4-phenylcyclohexane,” Iraqi Journal of Science, vol. 58, no. 4B, pp. 1998–2011, 2017.

[3] F. A. Omar, A. S. Hamad, and N. I. Taha, “Synthesis, characterization and evaluation antibacterial activity of some (1,3-oxazepine-4,7-dione and 1,3-benzooxazepine-4,7-dione) derived from sulphamethoxazole using irradiation method,” Kirkuk University Journal–Scientific Studies, vol. 17, no. 2, pp. 27–35, 2022.

[4] A. K. N. Allamy and S. A. Mejbel, “Preparation, characterization and biological activity of some new seven-membered heterocyclic compounds,” World Journal of Advanced Research and Reviews, vol. 15, no. 1, pp. 662–678, 2022.

[5] A. K. Khudhair Abbas and N. R. Jber, “Synthesis and characterization of new oxazepine compounds and estimation its biological activity,” Al-Nahrain Journal of Science, vol. 23, no. 3, pp. 17–23, 2020.

[6] N. S. Majeed, “Synthesis, evaluation of the biological activity and anti-oxidant for some heterocyclic compounds seven-membered rings derived from Schiff bases,” Journal of Kufa for Chemical Sciences, vol. 3, no. 2, pp. 415–434, 2024.

[7] R. Sheth, T. Thaker, S. Maurya, and A. Jyoti, “Synthesis, characterization, antimicrobial and antioxidant screening of novel oxazepines,” Indian Journal of Chemistry, vol. 64, no. 10, pp. 979–987, 2025.

[8] R. Faraj, A. J. Al-Safi, M. K. Al-hussainawy, and A. K. Abbas, “Novel 1,3-oxazepine-4,7-dione derivatives with antimicrobial anticancer and corrosion inhibition potential,” Discover Chemistry, vol. 3, Art. no. 2, 2026.

[9] R. F. Muslim, M. N. Owaid, A. M. Mohammed, H. M. Agha, N. F. Mazalan, N. M. B. Bahaudin, and M. I. N. Mohamad Isa, “Synthesis, characterization, ADMET, in silico molecular docking, biological activity of new oxazepine derivatives,” Journal of Molecular Structure, vol. 1351, pt. 2, Art. no. 144178, 2026.

[10] J. Eberhardt, D. Santos-Martins, A. F. Tillack, and S. Forli, "AutoDock Vina 1.2.0: New docking methods, expanded force field, and Python bindings," Journal of Chemical Information and Modeling, vol. 61, no. 8, pp. 3891–3898, 2021.

[11] O. Trott and A. J. Olson, "AutoDock Vina: Improving the speed and accuracy of docking with a new scoring function, efficient optimization, and multithreading," Journal of Computational Chemistry, vol. 31, no. 2, pp. 455–461, 2010.

[12] A. Daina, O. Michielin, and V. Zoete, "SwissADME: A free web tool to evaluate pharmacokinetics, drug-likeness and medicinal chemistry friendliness of small molecules," Scientific Reports, vol. 7, Art. no. 42717, 2017.

[13] A. Patan, M. Vijey Aanandhi, and P. Gopinath, "Molecular dynamics simulation approach of hybrid chalcone–thiazole complex derivatives for DNA gyrase B inhibition: Lead generation," RSC Advances, vol. 13, pp. 24291–24308, 2023.

[14] M. Bugnon, U. F. Röhrig, M. Goullieux, M. A. S. Perez, A. Daina, O. Michielin, and V. Zoete, "SwissDock 2024: Major enhancements for small-molecule docking with Attracting Cavities and AutoDock Vina," Nucleic Acids Research, vol. 52, no. W1, pp. W324–W332, 2024.

[15] Clinical and Laboratory Standards Institute, Methods for Dilution Antimicrobial Susceptibility Tests for Bacteria That Grow Aerobically, 12th ed., CLSI Standard M07. Wayne, PA, USA: CLSI, 2024.

[16] Clinical and Laboratory Standards Institute, Performance Standards for Antimicrobial Susceptibility Testing, 36th ed., CLSI Supplement M100. Wayne, PA, USA: CLSI, 2026.

[17] M. Brvar, M. Renko, A. Perdih, T. Solmajer, and D. Turk, "Crystal structure of the 24 kDa domain of Escherichia coli DNA gyrase B in complex with a small-molecule inhibitor (PDB ID: 4DUH)," Protein Data Bank, 2012.

[18] M. Brvar, A. Perdih, M. Renko, G. Anderluh, D. Turk, and T. Solmajer, "Structure-based discovery of substituted 4,5′-bithiazoles as novel DNA gyrase inhibitors," Journal of Medicinal Chemistry, vol. 55, no. 14, pp. 6413–6426, 2012.